SLAC-PUB-4649
May 1988
(E)

DESIGN AND PERFORMANCE OF THE ASP LEAD-GLASS CALORIMETER*

G. T. BARTHA,[a] D. L. BURKE, P. EXTERMANN,[b] P. H. GARBINCIUS,[c]
C. A. HAWKINS, M. J. JONKER,[d] L. KELLER, C. MATTEUZZI,[d]
N. A. ROE, AND T. R. STEELE
Stanford Linear Accelerator Center
Stanford University, Stanford, California 94309

and

A. S. JOHNSON, J. S. WHITAKER, AND R. J. WILSON
Boston University, Boston, Massachusetts 02215

and

C. HEARTY,[e] J. E. ROTHBERG, AND K. K. YOUNG
University of Washington, Seattle, Washington 98195

and

R. J. HOLLEBEEK
University of Pennsylvania, Philadelphia, Pennsylvania 19104

Abstract

The design of the ASP detector is described and details of the construction and performance of the lead-glass tracking calorimeter are presented. ASP, a non-magnetic particle detector, was used at the PEP e^+e^- storage ring at $\sqrt{s} = 29$ GeV to study low-multiplicity final states consisting primarily of electrons and photons. The design utilized extruded lead-glass bars to obtain a compact electromagnetic calorimeter with good energy resolution, tracking and pattern recognition capabilities.

Submitted to *Nuclear Instruments and Methods*

*This work was supported in part by the Department of Energy contracts DE-AC03-76SF00515, DE-AC02-86ER40284, and DE-AC02-76ER03071, and by National Science Foundation Grant PHY-8503215.

[a] Present Address: University of Southern California, Los Angeles, CA 90007
[b] Permanent Address: University of Geneva, Geneva, Switzerland
[c] Permanent Address: Fermi National Accelerator Laboratory, Batavia, Illinois 60510
[d] Present Address: CERN, EP Division, CH-1211
[e] Present Address: Lawrence Berkeley Laboratory, Berkeley, CA 94720

I. Introduction

The advantages of lead glass as a calorimeter element are well known: it has a high density, it transmits Čerenkov light in a frequency range which can be efficiently detected using common photocathode materials, and it can be obtained at modest cost in the form of extruded bars. We report here on the performance of a detector design that employed 632 extruded lead-glass bars to combine calorimetry and tracking. This device, the ASP detector, was operated for two years at the PEP e^+e^- storage ring at the Stanford Linear Accelerator Center. The complete apparatus consisted of a central lead-glass detector and a system of forward detectors which together covered the solid angle without any gaps or cracks above a polar angle $\theta > 21$ mr. The hermetic design allowed events with missing energy to be identified with high efficiency. The good position resolution of the lead-glass bars made it possible to distinguish between tracks that originated at the e^+e^- interaction point and those that did not, such as cosmic rays or interactions of the e^+ or e^- beams with residual gas in the vacuum pipe. The segmentation of the calorimeter was fine enough to provide good γ-π^0 discrimination for energies below a few GeV.

Following a brief description of the complete apparatus in Section 2, the design and construction of the lead-glass calorimeter is described in detail in Section 3. In Section 4 the data acquisition and trigger systems are described. Sections 5-7 comprise a detailed discussion of the offline calibration, energy determination and tracking of the lead-glass calorimeter. In Section 8 the performance of the lead-glass calorimeter is described, including energy, angular and timing resolution, and pattern recognition. Finally, a summary of the work is given in Section 9.

II. The Experimental Layout

The detector is shown schematically in Figs. 1 and 2. The lead-glass bars were arranged in four quadrants of five layers each. Alternating layers had 31 or 32 bars, staggered to eliminate cracks and to provide optimal position resolution. Viewed along the beam direction, $\hat{z}$, the pinwheel design left no radial gaps through which a charged particle or a photon from the interaction point could

escape undetected. This arrangement of the lead-glass bars, with the long axis of each bar perpendicular to the beam direction, provided spatial information in the xz or yz planes. Interleaved with the lead glass were five planes of proportional wire chambers (PWC). The PWC's were made from 2 m long aluminum extrusions with eight cells; four such extrusions formed one PWC plane. Each of the 32 cells in a plane measured 1.2×2.4 cm^2 and was strung with one 48 μm gold-plated tungsten sense wire. A mixture of 95% argon and 5% carbon dioxide gas flowed continuously through the PWC's at atmospheric pressure. The PWC wires were oriented with the sense wires parallel to the beam direction to provide spatial information in the xy plane, from which the azimuthal angle, ϕ, could be reconstructed. Taken together, information from the PWC's and lead-glass bars allowed for 3-dimensional track reconstruction.

A central tracker made of five planes of proportional chamber tubes detected charged particles between the beampipe and the lead-glass calorimeter. Each tube was 1.0×2.3 cm^2 in cross section and 2 m long. The walls were thinned by chemical etching to 0.3 mm to reduce the γ conversion rate. The tubes, which ran parallel to the beam, were staggered in the xy view so that charged particles from the beam axis could not pass completely undetected between them. Additional tubes were mounted in the corners to provide at least five layers of tracking at all values of ϕ. The tubes were glued together and mounted on a Hexcell backplate. Each tube was strung with a sense wire of resistive Stablohm 800 wire, and both ends were read out to provide a z-coordinate by charge division. The central tracker was operated with a gas mixture of 48.3% argon, 48.3% ethane and 3.4% ethyl alcohol vapor. The alcohol vapor was added to prevent degradation of the wires due to high radiation exposure near the beampipe. Surrounding the central tracker on all four sides was 2 cm of scintillator to provide redundancy in the identification of charged tracks. Each of the four veto scintillators was read out on both ends with a piece of wavelength shifter viewed by a single photomultiplier tube (PMT). The signals from both ends were used to reconstruct a z-coordinate.

The lead-glass bars, PWC's, central tracker and veto scintillators provided tracking and calorimetry for particles in the region $20° < \theta < 160°$. A system of forward detectors completed the coverage to within 21 mr of the beamline. Two

calorimeters were located on each side of the central detector, at $z = \pm 1.5$ m and $z = \pm 4.0$ m. The forward calorimeters (see Fig. 3) were constructed from alternating sheets of lead (0.6 cm) and scintillator (1.3 cm) in modules which were 6 radiation lengths (X_0) thick. The scintillator layers in each module were ganged together and read out by four wavelength shifter bars, each viewed by a single PMT. Two such modules were used for each of the inner calorimeters, which overlapped the angular region covered by the central detector and extended the coverage to within 100 mr of the beamline. Two crossed planes of PWC's, constructed of the same type of aluminum extrusion used for the central PWC's, were inserted between the modules to measure the spatial position of electromagnetic showers. The outer forward calorimeters, which covered the region between 21 mr and 120 mr from the beamline, consisted of three $6X_0$ modules each. PWC's were again located at a depth of $6X_0$, between the first and second modules. The additional material in the outer calorimeters reduced the probability that a photon would fail to convert in the detector, and provided good containment of showers from $e^+e^- \rightarrow e^+e^-$ at low angles. Between the inner and outer calorimeters on each side were drift chambers, located at $z = \pm 1.9$ m and $z = \pm 3.0$ m. At each location there were two drift-chamber planes to measure both the x and y coordinates, so as to provide charged particle tracking between 21 and 100 mr. The drift chambers were operated with a gas mixture of 48.2% argon, 48.2% ethane and 1.6% ethyl alcohol. The forward detectors provided a veto and calibration system for the ASP experiment as well as a luminosity monitor for the PEP storage ring.

Above the lead-glass calorimeter a time-of-flight (TOF) system consisting of 48 pieces of scintillator 3.45 m long, 20 cm wide and 2.5 cm thick was suspended from the ceiling. These counters were aligned with their long axes parallel to the beam direction in two overlapping groups which covered the lead-glass calorimeter in +z and -z. Each scintillator was read out on both ends, allowing reconstruction of the z coordinate. The TOF system was used primarily to reject cosmic ray events.

III. The Lead-Glass Calorimeter

The lead-glass bars measured $6 \times 6 \times 75$ cm^3 and were polished on both ends. The sides of the bars were smooth on an optical wavelength scale, but had ripples on the scale of a few mm which were created in the extrusion process. Extruded lead-glass bars are much cheaper to produce than polished lead-glass blocks, and it has been shown that their optical properties are equivalent.[1]

The lead glass used was Schott type F2; the composition is given in Table 1.

Table 1.

Lead glass composition

Element	Percentage Composition
Lead	41.8
Oxygen	29.7
Silicon	21.5
Sodium	3.7
Potassium	3.3
Cerium	0.35

This lead glass has a radiation length of 3.17 cm and an index of refraction of 1.58. It was doped with 0.35% cerium to increase its radiation hardness.[2] Menefee andThe presence of cerium causes the lead glass to become slightly yellow, reducing its transmission at short wavelengths, but it protects against the dramatic transmission losses which occur with large doses of radiation. This effect was measured using an intense ^{60}Co gamma ray source and one-inch cubes of lead-glass; the results are displayed in Fig. 5. For an integrated dose of 100 rad, undoped lead glass shows a 5% loss in transmission at $\lambda = 500$ nm (extrapolated to a length of 35 cm.) while lead glass with .3% cerium doping shows no loss after 100 rads. At greater exposures the transmission of undoped lead glass decreases rapidly while that of the cerium-doped lead glass decreases much more slowly.

Each lead-glass bar was read out on one end by an Amperex XP2212PC photomultiplier tube, a 12-stage PMT with high gain, good stability and low noise. The PMT's came with an attached printed circuit board base which had to be trimmed to 6×6 cm so that the lead-glass bars could be stacked without any gaps between them. Prior to assembly, the PMT's were calibrated using a green Hewlett-Packard Superbright (HLMP-3950) light-emitting diode (LED). In Fig. 6 the spectral response of the XP2212PC is compared to the Čerenkov spectrum, the spectrum from the calibration LED and the transmission spectra of doped and of undoped lead glass. The PMT's were powered by a single LeCroy 1440 high voltage supply, which was controlled by the on-line VAX via CAMAC. This programmable supply was monitored every four minutes to verify the voltage settings and could automatically correct voltages which drifted. It proved to be a very reliable, stable power supply. The PMT calibration data were used to select groups of eight PMT's with roughly similar response to be powered from a single high voltage channel. This voltage was fanned out through a resistive divider which was then adjusted to provide the correct voltage for each tube.

The PMT's were glued to the bars using Stycast 6061 optical epoxy; each PMT covered 42% of the surface area of the end of a bar. The bars were wrapped with aluminum foil on five sides and a μ-metal shield was put around each PMT to reduce the effect of external magnetic fields. The five lead-glass and PWC layers in each quadrant were then stacked in a light-tight box made of 0.75 inch thick aluminum. To minimize the non-active material inside the lead-glass calorimeter, the walls of the aluminum box were made half as thick where two quadrants abut. The calorimeter was supported internally by 6.8 cm high aluminum I-beams. Between adjacent layers of PWC six I-beams were used as spacers, creating 'shelves' on which the lead-glass bars were placed between thin layers of foam padding. This was necessary because some of the lead-glass bars were slightly bowed, with a maximum deviation from linearity of 2 mm. This was an artifact of the extrusion process; the bowing occurred only in the horizontal plane as the bars were extruded onto a flat surface. To avoid any small gaps, the bars were stacked with their straight sides together. The weight of the lead glass was then borne by the PWC's and I-beams, and any curvature in the bars was accommodated by the

extra height of the I-beams. This arrangement prevented undue stress on the lead-glass bars and bowing of the PWC planes.

Each quadrant measured approximately $1.0 \times 0.5 \times 2.0$ m^3 and was an independent unit which was easily dismounted and transported. This was a necessary part of the design, because access to the PEP interaction region where the ASP detector was installed was restricted: every component had to be carried in along the arcs from an adjacent interaction region. The two lower quadrants were mounted on rails and each was then bolted to the quadrant above, allowing the detector to be split by a remotely-controlled hydraulic drive. This provided easy access to the beampipe and detector components whenever necessary. The ASP detector was located directly downstream from the PEP electron injection port, so to avoid excess radiation damage the two halves of the detector were moved away from the beamline whenever electrons were injected into the storage ring. To further protect the lead glass during injection, lead-brick walls were installed to shield it when it was in the open position. Electronic sensors ensured that the two halves were in the fully-closed position for data taking.

The PMT's were monitored online with LED's of the same type as was used in the initial calibration. There was one LED per quadrant, each of which could be pulsed by a high-current pulser.[3] The light pulses were transmitted to each PMT with a light fiber. One end of each light fiber was embedded in the epoxy used to glue the PMT's to the lead-glass bars. The output of each LED was monitored by a reference PMT which also viewed a small NaI(Tl) scintillator crystal doped with ^{241}Am[4] which served as a stable light source.[5] This system was used to provide a relative calibration of the PMT's for checking their stability during data taking. It was not used for an absolute calibration as the transmission of the light fiber connections drifted with time, and also the LED spectrum did not cover the full range of the PMT photocathode spectral sensitivity. The reliability of the phototubes was high: fewer than 1% of the tubes failed for any reason over the entire course of the experiment.

IV. Data Acquisition and Trigger

The signals from each of the 632 PMT's used to read out the lead-glass bars were first sent through a passive transformer splitter. One of the two resulting signals was sent to a SHAM-BADC system,[6] a sample-and-hold module followed by an analog-to-digital converter which also performed pedestal subtraction and gain correction. This provided the primary read-out of the calorimeter. The other half of the signals were summed, first in groups of eight from adjacent bars in the same layer, then with the other groups of eight in each layer to form 20 analog signals, one from each of the five layers in the four lead-glass quadrants.

The layer sums were then fanned out; see Fig. 4. One copy was digitized and read out to provide a redundancy check against the SHAM-BADC system. It was also used in the offline code to correct for saturation in the BADC, which occurred when more than about 1.2 GeV was deposited in a single bar. Another copy was summed to provide the total quadrant signals, which were summed in turn to form an analog signal proportional to the total calorimeter energy. These sums were also digitized and readout. A third copy of the layer sums was integrated and discriminated, as were the quadrant and total lead-glass sums, to provide digital inputs for the trigger logic.[7]

The ASP trigger decision was based on the discriminated signals from the layer, quadrant and total lead-glass sums, together with discriminated signals from the FSC's and veto scintillators. These digital inputs were sent to two Memory Logic Units (MLU's), which functioned as flexible look-up tables which could be programmed to recognize desired combinations of logical inputs from the various detector elements. The summary outputs from the MLU's were fed into the input latches of the Global Control module (GC), which would initiate digitization and event read-out by the host VAX 11/750 computer. The trigger decision was made within $1\,\mu$s, which is less than the $2.4\,\mu$s between successive beam crossings in the PEP storage ring to avoid dead time. The event readout required about 10 ms. Upon completion of the readout, the VAX re-enabled the GC so it was ready for the next event. The GC was driven by the PEP RF clock during normal data-taking to synchronize the trigger and data acquisition systems with the beam crossing. It could also be run from a free-running oscillator

for test purposes. A detector monitoring system which continuously checked all voltages, currents, gas composition, etc. was also connected to the GC so that when a malfunction was detected the GC would immediately declare a fault and suspend data acquisition.

The simplest trigger fired when the total signal from the lead-glass calorimeter exceeded a pre-determined threshold. This threshold, which was set at 1.5 GeV, was determined by the requirement that it be greater than the coherent noise, which was insignificant on individual channels but became large when summed over all 632 channels. The segmentation of the calorimeter and the successive summing of the lead glass signals made sums from individual layers and quadrants available for use in more sophisticated triggers with lower thresholds, without increasing the trigger rate above manageable levels. For example, special triggers were designed to detect events with a single photon in the lead glass. A threshold of .7 GeV total energy was achieved by requiring that at least .15 GeV be deposited in the back four layers of one and only one quadrant, no more than two veto scintillators fired, and less than 1 GeV was deposited in the FSC's. These additional requirements reduced the contribution from beam-gas interactions. A variation on this trigger required that two opposite quadrants had at least .15 GeV in the back four layers, a topology which was typical for an interesting class of two-photon events. Another trigger which was designed to log out radiative Bhabha events required at least 0.3 GeV in the lead glass plus a coincidence between two FSC's with at least 7 GeV on either side of the detector. In addition there were diagnostic triggers which logged out cosmic rays, random beam crossings, and low-angle Bhabhas for luminosity studies. The total trigger rate of the ASP detector was typically 4.5 Hz. The precise value varied depending upon the specific luminosity and beam steering in PEP, but was never over 7 Hz, which was within the capabilities of the data acquisition system.

V. Off-line Calibration of the Lead-Glass Calorimeter

Cosmic ray muons which traversed the lead-glass calorimeter were used to perform an off-line calibration of the PMT response. These events were continuously recorded by a special trigger which fired when a charged particle was

detected in the veto scintillators surrounding the central tracker in a 15 ns time window ending 5 ns before the beam crossing. This sample was tracked and the signal deposited in each bar was corrected for path length. The average path-corrected signal displayed a strong dependence on both the distance of the track from the PMT and on the angle of the track with respect to the long axis of the bar (Fig. 7). The dependence on distance was due to reflection losses and attenuation of the signal in the lead glass, modified by geometry- and frequency-dependent increases in light collection when the distance became less than a few cm. The dependence on angle was due to the fact that the Čerenkov light generated by a particle traveling towards the PMT travels a shorter distance in the lead glass than light generated by particles heading away from the PMT, which must travel to the far end and be reflected back. A change in direction also changed the angle of incidence of the light as it traveled down the bar by internal reflection and hence changed the total distance traveled in the glass.

Each lead-glass quadrant was oriented in a different direction, with some PMT's pointing up, some down and others oriented horizontally. Therefore the angular distribution of the predominantly down-going cosmic rays with respect to the axis of the lead-glass bars was different in each quadrant. This resulted in a different average path-length corrected signal, due to the attenuation effects described above. To compensate, another correction had to be applied on an event-by-event basis. The correction factor was a function of both the distance of the track from the PMT and the angle of the track with respect to the bar, taken from a look-up table compiled from plots such as those in Fig. 7. The peak was extracted from the resulting spectrum for each PMT and this value was used to normalize its response.

This cosmic-ray calibration was more accurate than the one which had been performed with an LED prior to installation because the spectral response of the PMT's was integrated over the correct frequency range of Čerenkov light. In addition, any channel-to-channel variation in the electronics used to read out the PMT's was automatically included in the calibration. This calibration was also used to check for evidence of radiation damage, which would cause a time dependent decrease in the transmission of the lead-glass bars. No significant

decrease in response was observed. Over the two-year period when the ASP detector was installed at PEP, more than 1 kilorad of gamma radiation and an equal dose in neutrons were recorded by dosimeters affixed to the exterior of the lead-glass calorimeter on the side nearest the beampipe. Dosimeters attached to fixed supports near the beampipe which were not retracted during injection recorded much higher levels. Although a large fraction of the gamma rays must have been absorbed by the 0.75 inch aluminum box surrounding the lead glass, a significant number of neutrons would have penetrated into the calorimeter. Moving the detector away from the beampipe during injection and the installation of lead-brick walls were responsible for a significant reduction in the integrated radiation dose seen by the lead glass, and the addition of cerium to the lead glass prevented any significant damage from the radiation which was absorbed.

VI. Energy Determination in the Lead-Glass Calorimeter

The Čerenkov light collected from an electromagnetic shower in lead glass is proportional to the integrated path length traveled by all charged particles in the shower which are above the Čerenkov threshold (0.7 MeV for electrons), and is therefore proportional to the energy of the shower. The light is transmitted by internal reflection down the bar to the PMT, and undergoes some attenuation in this process. To correct for this attenuation, a look-up table identical to the one used to correct cosmic-ray signals in the off-line calibration was used. The correction was applied after the event was tracked, using the track parameters to calculate the angle and distance of the shower from the PMT. An attempt was made to improve the attenuation correction by applying it to every charged particle in electromagnetic showers simulated with the EGS Monte Carlo program.[8] By this procedure an energy-weighted average was made over the spatial and angular distribution of all the particles in a shower. However this 'improved' attenuation function gave slightly worse resolution when applied to the data, for reasons which were not fully understood, and was not used.

Further corrections were made for leakage, pre-radiation and the absorption of energy in the non-active material inside the calorimeter. The amount of energy which leaks out of the calorimeter is a function of the total thickness (in radiation

lengths) and the incident particle energy. Using EGS the following empirical approximation was derived to correct for leakage on the mean:

$$E_{leak} = 2.0 \times e^{-.3X} \times {E_{inc}}^{1.4} \text{ GeV} \quad (1)$$

where E_{leak} is the energy lost in GeV, X is the thickness of the detector in radiation lengths along the trajectory of the track, and E_{inc} is the incident energy in GeV. A weighted average over the spatial extent of the shower was used to calculate X; a gaussian with $\sigma = 5°$ was used for weighting. The thickness of the detector varied from 10 X_0 at normal incidence to 20 X_0 at $\theta = 30°$. The thinnest part of the detector was in the corners between quadrants, where X $\simeq$ 9 X_0 at $\theta = 90°$. For photons, the estimated point of conversion in the lead glass was also used in the calculation of X. A first estimate of E_{leak} was obtained by substituting the observed energy for E_{inc}, then $E_{obs} + E_{leak}$ was substituted for E_{inc} and this procedure was iterated until the estimate of E_{leak} converged to within 5% of the previous estimate for E_{leak}. For a 1 GeV particle at normal incidence, the mean energy lost is about 100 MeV, or 10%, and at $\theta = 30°$ this is reduced to 0.5%. The corresponding numbers for a particle of 14.5 GeV are 30% and 1.5%. This correction is clearly most important at wide angles. No attempt was made to take into account fluctuations in leakage.

Radiation of charged particles in the material preceding the calorimeter and absorption of energy in the non-active material have also been studied using EGS. At normal incidence a particle will traverse 0.36 X_0 before entering the lead-glass calorimeter. This is primarily due to the 0.75 inch thick aluminum box enclosing each quadrant. A 1 GeV charged particle deposits on average 20 MeV in this material. The pre-radiation increases exponentially with radiation length and there is also a weak dependence on the energy of the incident particle. To correct for this loss, the following empirical formula was developed using EGS simulation:

$$E_{pre} = .008 \times e^{2.6X} \times e^{.04E_{inc}} \text{ GeV} . \quad (2)$$

In this formula, E_{pre} is the amount energy deposited in GeV, X is the amount of material in radiation lengths traversed before entering the lead glass, and E_{inc} is again the incident particle energy in GeV.

Energy is also absorbed in the Al walls of the PWC's, the I-beams, and most importantly, the 0.75 inch of aluminum between quadrants. The correction for this energy loss is a strong function of ϕ, and becomes largest when a track is heading directly between two lead-glass quadrants. Using EGS, the ϕ dependence was mapped out and a look-up table was constructed. The fraction of energy absorbed relative to the total incident energy is roughly constant with energy, and varies from 4.5% at normal incidence to 12% at $\phi = 60°$, which is approximately where the boundary between quadrants is located.

VII. Tracking with the Lead Glass

The tracking proceeded in several stages. The boundaries of each shower were first determined with a cluster-finding algorithm. Fluctuations in the development of an electromagnetic shower create gaps in the pattern of energy deposition, while on the other hand two showers which are close together in the plane of a quadrant may overlap. The clustering algorithm therefore allowed gaps, but was also sensitive to peaks and valleys and would start a new cluster when large enough fluctuations in signal were encountered. Clusters were not continued across quadrant boundaries; clusters from a single shower which extended into adjacent quadrants were combined at a later stage of the tracking.

A two-dimensional total least squares fit was then performed for each cluster. This fit found the axis about which the sum of the squares of the perpendicular distances to each bar, D_i, was minimized. The signal in each bar corrected for PMT gain, S_i, was used to weight each term. (The attenuation correction could not be applied at this stage because the angles of the track were not yet determined.) The quantity to be minimized was:

$$M_{W^2} = \sum_i S_i D_i^2 \quad . \tag{3}$$

A slope and intercept in the plane of the quadrant (xz or yz) were extracted from this fit.

The signals observed in the central PWC's, the central tracker, and the forward systems were all tracked independently and combined with the lead-glass clusters to reconstruct an event topology. To accomplish this, the track segments from each system were reduced to vector and error matrices. A topology finding routine then identified the segments from each system which could belong together in a track. A least-squares fit was performed, and if the χ^2 was satisfactory a track was created utilizing all the information from the various systems. If the χ^2 was unsatisfactory, the segment which contributed the most to the χ^2 was dropped and the fit was tried again. Clusters from a shower which crossed the boundary between two quadrants were combined in a similar fashion. The clusters were required to match based on a χ^2 formed from their θ values and errors, and information from the other central tracking systems was used in the fit. Tracks from minimum-ionizing particles were treated in the same way as electromagnetic showers; the tracking code worked equally well for both.

Ambiguities arose in matching lead-glass clusters and PWC clusters when there were multiple tracks per quadrant. For charged tracks this could usually be resolved by the central tracker. However, if there were multiple neutral tracks in a quadrant, the tracking algorithm had to rely on a comparison of the signal deposited in each layer of the lead glass and PWC clusters. From this comparison a χ^2 was extracted which indicated how well the patterns of energy deposition in the two systems matched. When two showers had very different patterns this method worked well; however if they were similar it was difficult to correctly assign the PWC clusters to the lead-glass clusters. Because of this limitation the tracking worked best for low multiplicity events.

VIII. Performance

In this section we discuss the performance of the ASP lead-glass calorimeter, including energy resolution, angular resolution and $\gamma - \pi^\circ$ discrimination. One of the most important tools developed for performance studies of the detector was kinematic fitting of $e^+e^- \rightarrow e^+e^-\gamma$ events. A sample of approximately

8×10^4 of these radiative Bhabha events was selected in which two of the outgoing particles were between 21 and 180 mr from the beamline, where the long lever arm of the forward systems afforded a precise measurement of their position. The third particle, either an electron or photon, was required to be in the lead-glass calorimeter. The energy of the track in the lead glass was kinematically limited to less than about 4 GeV for this class of events. The events were fitted using the kinematic-fitting program SQUAW.[9] Because the center-of-mass energy in e^+e^- collisions is known ($\sqrt{s} = 29$ GeV at PEP), the fit to a three-particle final state was over-constrained and the detector performance could be studied by removing the variable of interest from the fit.

In particular, the absolute energy scale of the lead-glass and the forward calorimeters was determined by including just the angles of all three tracks in a one-constraint fit and extracting the energies. Once the overall normalization had been established, the calorimeter resolution was determined by plotting the difference between the measured energy and the fitted energy. The results for the lead glass are displayed as a function of energy in Fig. 8. The curve is well described by the resolution function

$$\frac{\sigma_E}{E} = \frac{10.0\%}{\sqrt{E}} \,. \tag{4}$$

This resolution was achieved using the corrections already described for attenuation, leakage and pre-radiation.

Bhabha events were used to study the angular resolution of the lead glass. The quantity which is actually measured with the lead-glass calorimeter is θ_p, the polar angle projected into the xz or yz plane. The resolution in θ_p improves at lower angles because the lever arm is greater as the distance to the interaction point increases. This dependence is displayed in Fig. 9, where the beam-spot constrained resolution of θ_p is plotted as a function of θ_p, measured with showers of 14.5 GeV. The resolution averaged over all angles is $\sigma = 1.9°$. The angular resolution of the lead glass was also a function of energy, becoming worse at lower energies because the position of the shower centroid was less well measured. For showers from radiative Bhabha events, ranging in energy from 0.5 to 3 GeV, the average resolution was $\sigma = 4.4°$.

The spatial origin of a shower in the lead glass was characterized by the distance of closest approach to the beamspot in the xz or yz plane, R_z. This quantity was used because the resolution is then approximately independent of θ_p. For 14.5 GeV showers from Bhabha events the R_z distribution was Gaussian, with an average resolution of $\sigma = 2.6$ cm. The resolution is shown as a function of θ_p in Fig. 10. For low-energy showers, such as those from radiative Bhabha events, the distribution was Gaussian with $\sigma = 2.8$ cm and a small exponential tail.

Timing information from the lead glass was obtained for each quadrant, and corrections were applied using the tracking information. Both the path length of the track from the interaction point to the lead-glass calorimeter and the distance the light traveled down the bar to the PMT were taken into account. After these corrections were applied the timing resolution was $\sigma = 1.2$ ns for a 1 GeV shower and $\sigma = 1.0$ ns above 2.5 GeV.

The ability to discriminate between γ's and π°'s using the lead-glass calorimeter depended on the opening angle between the two photons from the π° decay, which was a function of the π° energy. Above 3 GeV the minimum opening angle was less than 5° and very little discrimination was possible. At lower energies, if the two γ's were well separated in the lead glass the invariant mass of the π° could be reconstructed. When they overlapped, pattern recognition could be used to identify the broader shower which resulted.

The case in which both γ's were reconstructed in the lead glass was studied using the two-photon reaction $e^+e^- \to e^+e^-\gamma\gamma \to e^+e^- f_2(1270)$, with subsequent decay of the f_2 into $\pi^\circ\pi^\circ$. Untagged events with three or four reconstructed photons in the lead glass were selected (allowing one π^0 to be merged). The total invariant mass distribution for these events is shown in Fig. 11; clear evidence for production of the f_2 is seen, as well as substantial continuum production of $\pi^\circ\pi^\circ$ below it. The lower end of the distribution is cut off by trigger inefficiency. The invariant mass of all photon pair combinations is shown in Fig. 12a; a π° peak is seen above a combinatorial background. To eliminate most of this background, events with only three photons were chosen : one π° was assumed to be merged in the lead glass and the other was identified by choosing the two

photons with the smallest azimuthal separation. The invariant mass distribution for the photon pairs chosen using this hypothesis is plotted in Fig. 12b. A substantial improvement is seen. The mass resolution is about 30 MeV and the mean value is $127 \pm .5$ MeV. The peak is shifted down from the known π° mass of 135 MeV because of a systematic underestimatation of the opening angle between the photons in the xy plane. Since these events were selected to have photons which were well-separated in the lead glass, they were more likely to overlap in xy, the plane of the central PWC's. When only one cluster was reconstructed in the PWC's it was matched to both lead-glass clusters by the tracking code, so both photons would be assigned the same value of ϕ. Another problem was inefficiency in the central PWC system for low-energy photons. The efficiency to have a PWC cluster was measured to be $> 99\%$ for electron or photons above 1 GeV, 90% at 0.5 GeV, and 60% at .2 GeV. In an asymmetric decay, where one of the γ's from the π° had much less energy, it could fail to create any hits in the PWC system and be assigned to the PWC shower created by the more energetic γ by default. Requiring that both photons have distinct PWC clusters assigned to them results in the invariant mass plot of Fig. 12c. The mean value of the invariant mass peak is now 136 ± 1.0 MeV, consistent with the π° mass.

To identify π°'s which were merged in the lead glass, two moments of the shower were calculated using the quantities D_i, the perpendicular distance from the i'th bar to the shower axis, and L_i, the depth of the i'th bar in the shower. The moments were then obtained as:

$$\begin{aligned} M_{W^2} &= \frac{1}{\sum_i E_i} \sum_i E_i D_i^2 \\ M_{LW^2} &= \frac{1}{\sum_i E_i} \sum_i E_i D_i^2 (L_i - \bar{L}) \quad . \end{aligned} \tag{5}$$

The sum was over all bars with significant energy. E_i was the energy corrected for both PMT gain and attenuation, and $\bar{L}$ was the average depth of the shower, defined as:

$$\bar{L} = \frac{1}{\sum_i E_i} \sum_i E_i L_i \quad . \tag{6}$$

The first quantity, M_{W^2}, was larger for broad showers such as those initiated by π°'s. The M_{LW^2} moment was used to discriminate against showers which had uneven longitudinal development.

The use of these moments to reject π°'s is illustrated by again using data from two-photon interactions. In Fig. 13a the invariant mass of selected events with two 'photons' in the lead glass is plotted. (For comparison, the selection criteria are identical to those used in Fig. 11, except for the requirement that two photons, rather than three or four, be found.) Contributions from two-photon production of the η (M = .549 GeV) and η' (M = .958 GeV) mesons, with subsequent decay into two photons, are present. However the η' peak is difficult to separate from the broad $f_2(1270) \rightarrow \pi^\circ\pi^\circ$ peak (Γ_{tot} = 176 MeV), where both π°'s overlap in the lead glass. In Fig. 13b, an additional requirement has been imposed, rejecting events in which either photon has a large M_{W^2} in the lead glass. Suppression of the f_2 is achieved with good efficiency for the η and η'. Finally, in Fig. 13c, events with a large M_{W^2} in the central PWC's have also been rejected, resulting in a further improvement of the η' signal.

The efficiency of the moments cuts for rejecting π°'s while retaining γ's is a function of energy. This energy dependence was studied using γ's and π°'s generated using EGS; the results are shown in Fig. 14 where the percentage of events which would fall below a given cut in M_{W^2} is plotted vs M_{W^2} at energies of 1 and 2 GeV. Additional discrimination can be gained by calculating similar moments for the central PWC's, which are orthogonal to the lead-glass bars and can identify those π°'s in which the two photon showers line up along the axis of the lead-glass bars. Application of the two moments cuts on both the lead glass and the central PWC systems rejected 91% of beam-gas π°'s with transverse momentum greater than 0.8 GeV/c in the region $20^\circ < \theta < 160^\circ$, while retaining 86% of the photons.

IX. Conclusions

The design and construction of a compact, hermetic lead-glass detector well-suited for detecting low-multiplicity events consisting primarily of electrons and photons has been described. No radiation damage was observed in the lead

glass over a period of two years of operation at the PEP storage ring. Extruded lead-glass bars have been shown to work well as both calorimetric and tracking elements.

We thank D. Chambers, R. Baggs, D. Forbush, T. Lyons, C. Noyer, K. Skarpass, R. Stickley and F. Toevs for considerable technical assistance with the construction and installation of the detector. We are also grateful to the PEP operations staff.

REFERENCES

1. P. Grannis, D. Jaffe and M. Marx, Nucl. Instr. and Meth. **188** (1981) 239.

2. P. Levy *et al.*, Jour. Am. Ceram. Sos. **57** (1974) 176.

3. The pulser used was similar to that described by L. R. Fortney in *Proceedings of the Calorimeter Calibration Workshop*, edited by H. Jostlein (Fermi National Accelerator Laboratory, Batavia, Illinois, 1983), p. 1.

4. J. Menefee and Y. Cho, IEEE Trans. Nucl. Sci. **NS-12** (1966) 159.

5. J. S. Beale *et al.*, Nucl. Instr. and Meth. **117** (1974) 501.

6. E. Cisnero *et al.*, IEEE Trans. Nucl. Sci. **NS-28** (1981) 465; M. Breidenbach *et al.* IEEE Trans. Nucl. Sci. **NS-25** (1978) 706

7. For details of the ASP trigger system, see: R. J. Wilson, *Proceedings of the Workshop on Triggering, Data Acquisition and Computing for High Energy/High Luminosity Hadron-Hadron Colliders*, edited by B. Cox, R. Fenner and P. Hale (Fermi National Accelerator Laboratory, Batavia, Illinois, 1986), p. 118.

8. R. L. Ford and W. R. Nelson, "The EGS Code System: Computer Programs for the Monte Carlo Simulation of Electromagnetic Cascade Showers (Version 3)," SLAC-PUB-0210, June 1978.

9. O. Dahl *et al.*, Lawrence Berkeley Laboratory, Group A Programming Note # P-126, July 1968.

FIGURE CAPTIONS

1. Side view of the ASP detector. The apparatus is 8.8 m long and 1.2 m wide. The coordinate system used is shown.

2. Cross section in the xy plane of the central calorimeter and tracking system. Only a section of the central tracker is shown; it completely surrounds the interaction point (IP).

3. Front and side views of a forward shower counter module. The inset shows details of the construction of a corner of the module.

4. Analog summing circuits and trigger schematic.

5. Effect of ^{60}Co γ radiation on transmission of light through samples of a) undoped lead glass and b) lead glass with .3% cerium doping. Curve A is before exposure to radiation, B is after 1.2×10^2 rads, C is after 1.2×10^3 rads, D is after 1.2×10^4 rads and E is after 5.0×10^4 rads of γ radiation.

6. Comparison of internal transmission curves for 2.54 cm samples of doped and undoped lead glass (solid lines) with the Čerenkov spectrum (dashed line), the spectral sensitivity of the Amperex XP2212PC photocathode (dash-dotted line) and the relative spectral output of the HLMP-3950 LED (dotted line).

7. Attenuation of Čerenkov light in the lead-glass bar, as a function of length along the bar, measured with minimum ionizing tracks from cosmic rays. In a) the tracks are at an angle $\alpha = 45°$ with respect to the bar, pointing toward the PMT. In b) $\alpha = 135°$, pointing away from the PMT.

8. Energy resolution of the lead glass as a function of energy, measured using kinematically-fitted radiative Bhabha events.

9. Angular resolution of the lead glass measured using Bhabha events. θ_p is the polar angle projected into the xz or yz plane.

10. Resolution of the lead glass on the distance of closest approach to the origin, R_z, plotted vs θ_p as measured using Bhabha events.

11. Invariant mass distribution of selected events with three or four clusters in the lead glass.

12. a)Invariant mass distribution of all photon pairs for the event sample used in Fig. 11. In b), three-photon events were chosen and the invariant mass of the pair with the smallest azimuthal separation is plotted. In c), the additional requirement is made that both photons have a separate PWC cluster to measure ϕ.

13. a) Invariant mass distribution of selected events with two photons in the lead glass. b) Same event sample, with the requirement that neither photon have a large width (M_{W^2}) in the lead glass. c) Same as b), with the additional requirement that neither photon have a large width (M_{W^2}) in the central PWC's.

14. Percent of π^0's (crosses) and γ's (dots) passing M_{W^2} cut as a function of M_{W^2} at an energy of a) 1 GeV and b) 2 GeV.

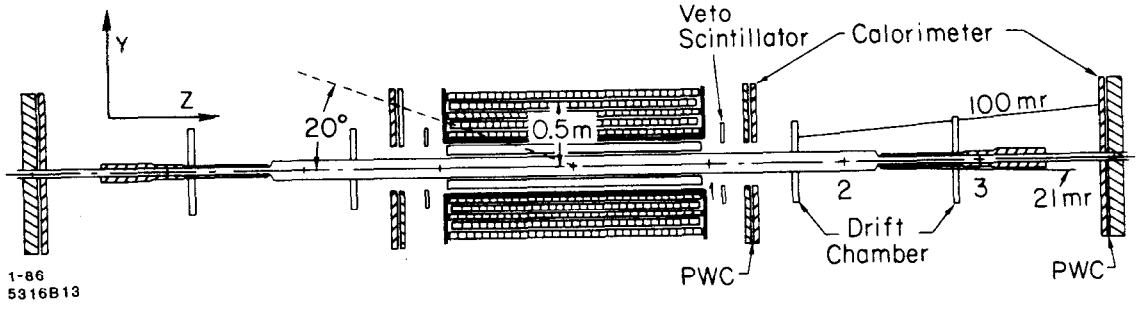
Y
Z
20°
0.5m
Veto
Scintillator
Calorimeter
100 mr
21 mr
1
2
3
Drift
Chamber
PWC
PWC
1-86
5316B13

Fig. 1

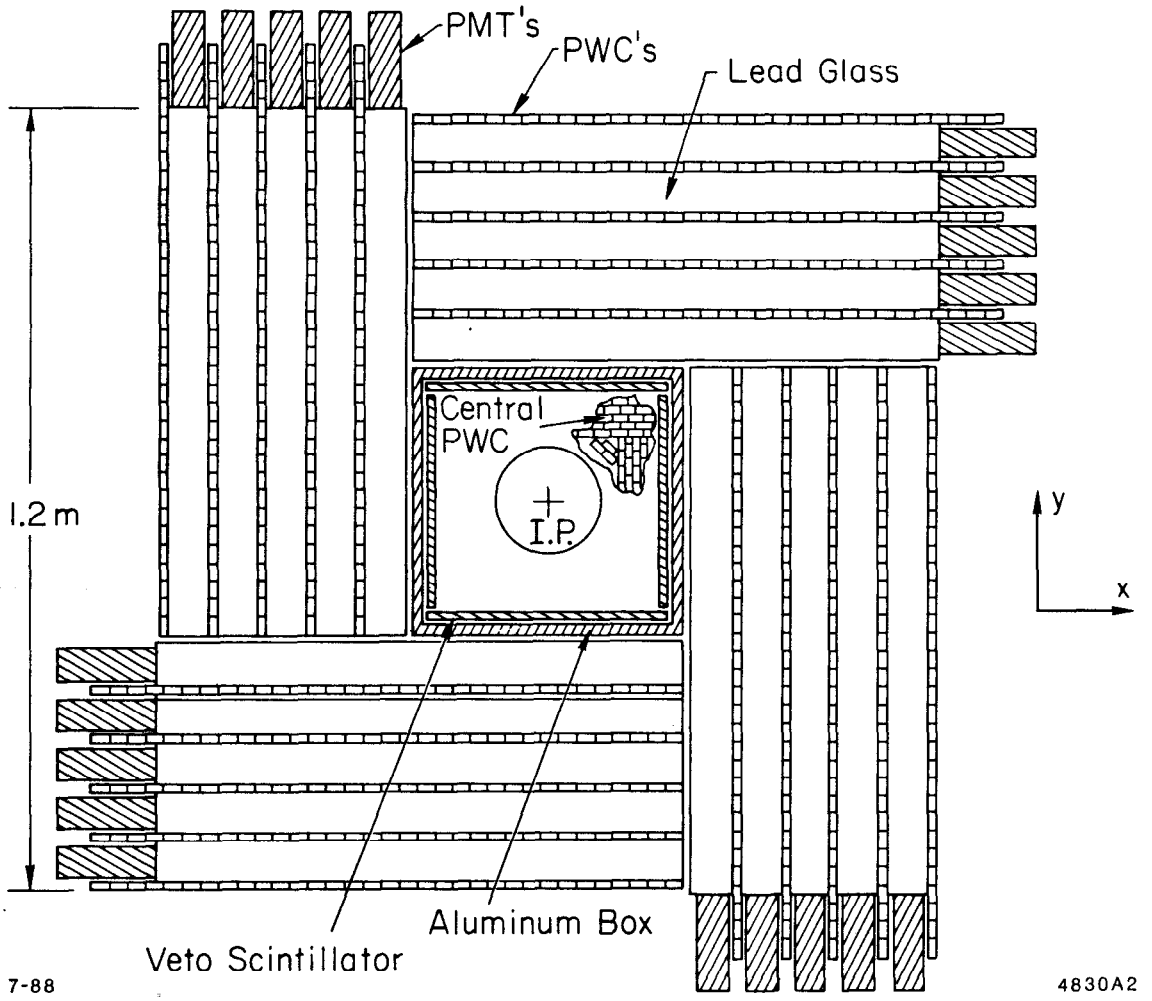
PMT's
PWC's
Lead Glass
Central
PWC
I.P.
1.2 m
y
x
Aluminum Box
Veto Scintillator
7-88
4830A2

Fig. 2

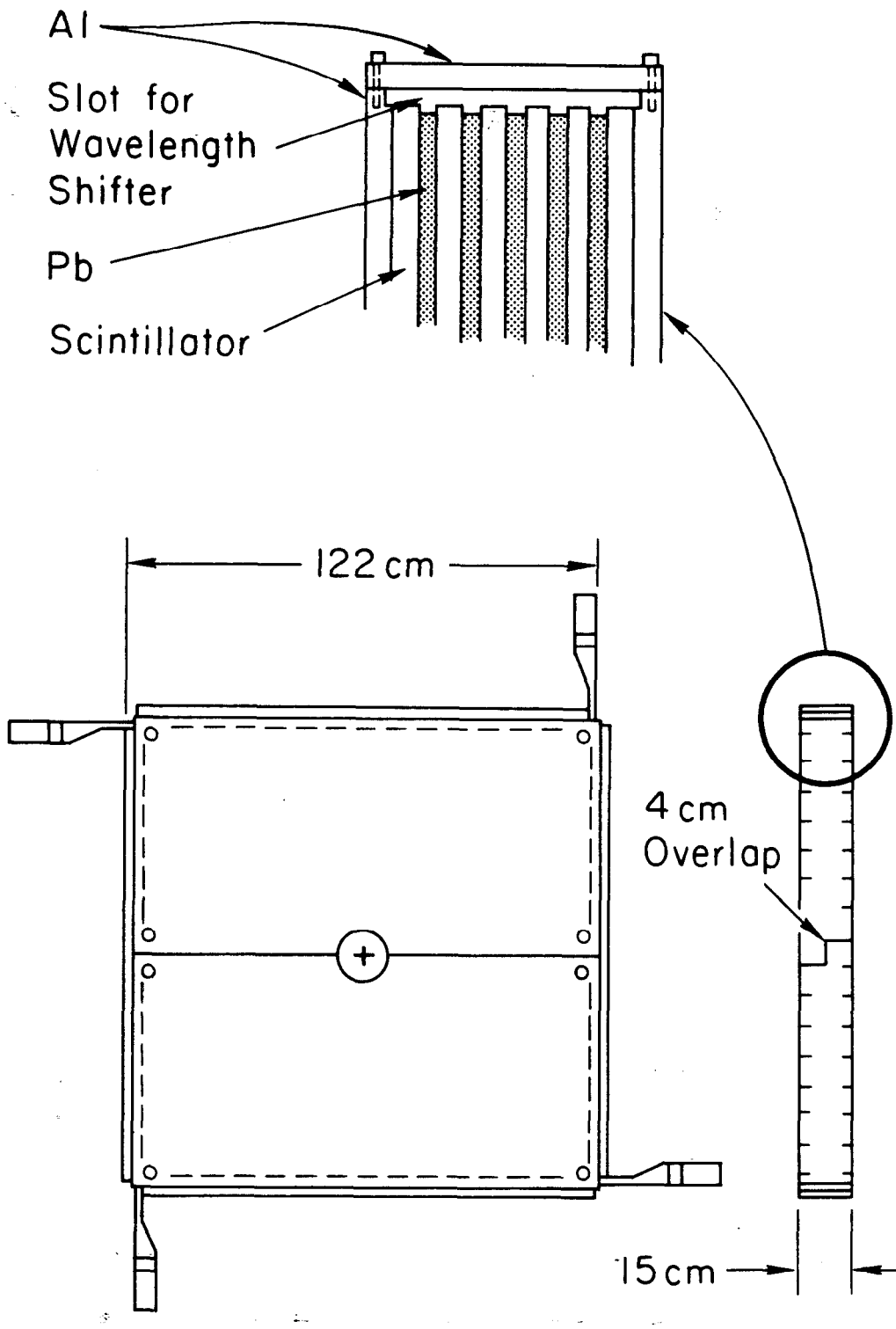
Al
Slot for
Wavelength
Shifter
Pb
Scintillator
122 cm
4 cm
Overlap
15 cm
7-88
4830A5

Fig. 3

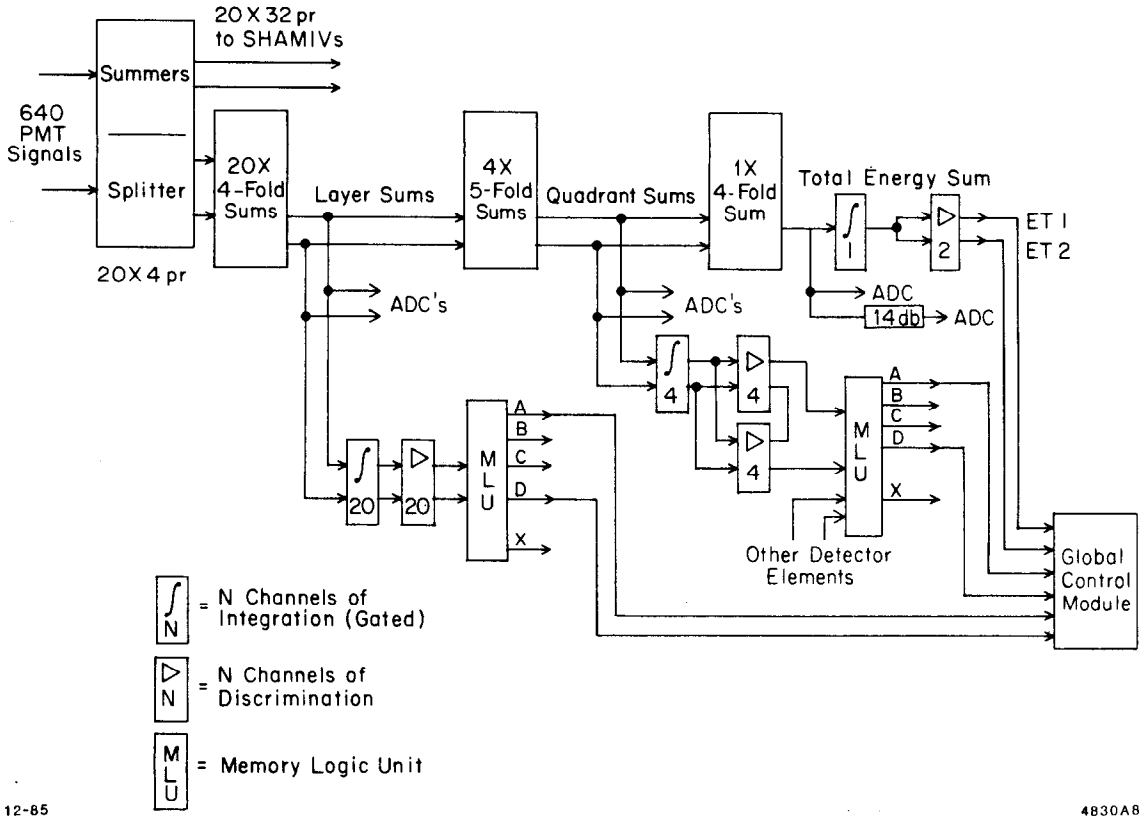
20 X 32 pr
to SHAMIVs
Summers
640
PMT
Signals
Splitter
20X4 pr
20X
4-Fold
Sums
Layer Sums
4X
5-Fold
Sums
Quadrant Sums
1X
4-Fold
Sum
Total Energy Sum
ET 1
ET 2
ADC's
ADC's
ADC
14 db
ADC
20
20
M
L
U
A
B
C
D
X
4
4
4
M
L
U
A
B
C
D
X
Other Detector
Elements
Global
Control
Module
= N Channels of
Integration (Gated)
= N Channels of
Discrimination
= Memory Logic Unit
12-85
4830A8

Fig. 4

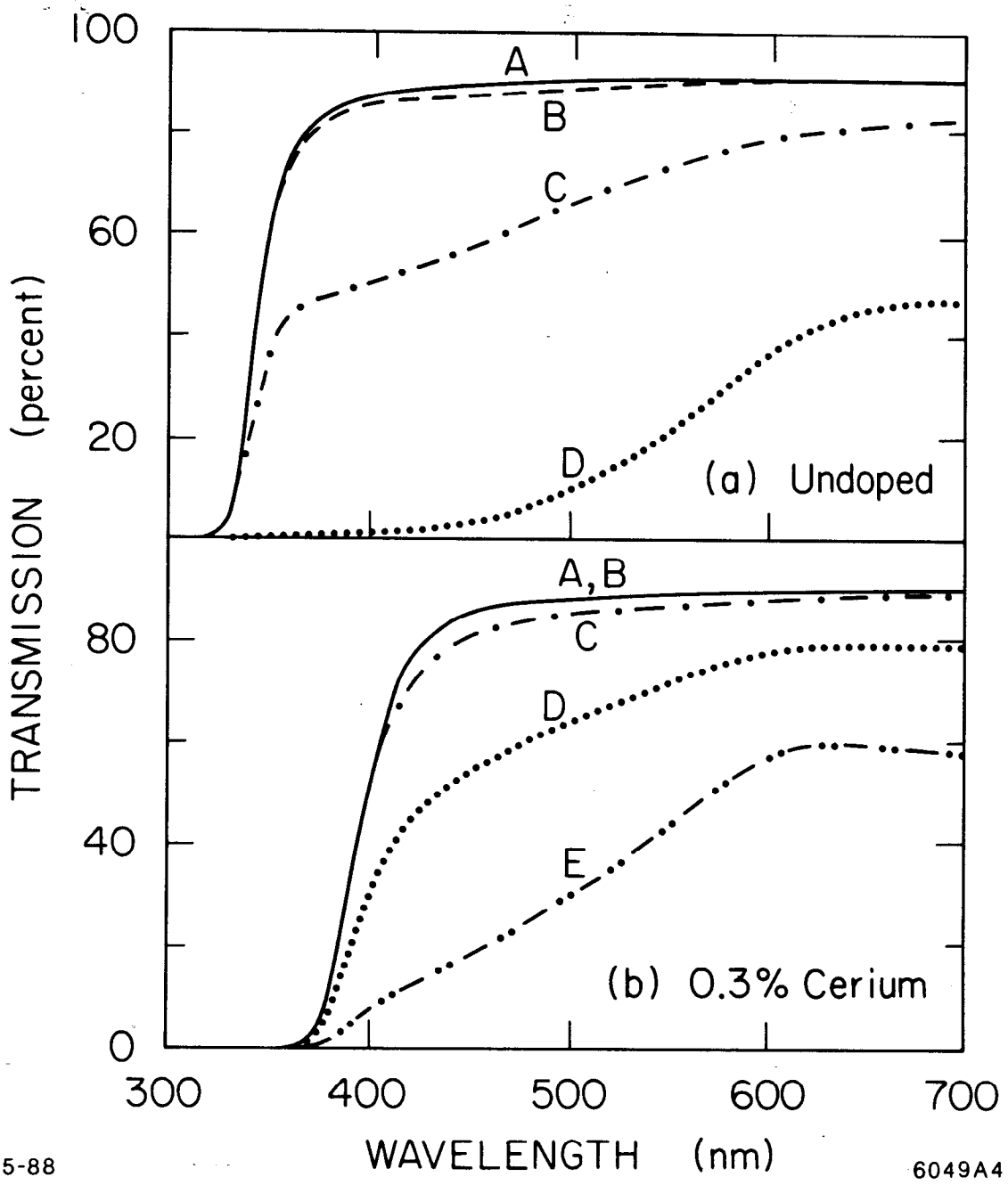
100
60
20
0
80
40
A
B
C
D
(a) Undoped
A, B
C
D
E
(b) 0.3% Cerium
TRANSMISSION (percent)
300
400
500
600
700
WAVELENGTH (nm)
5-88
6049A4

Fig. 5

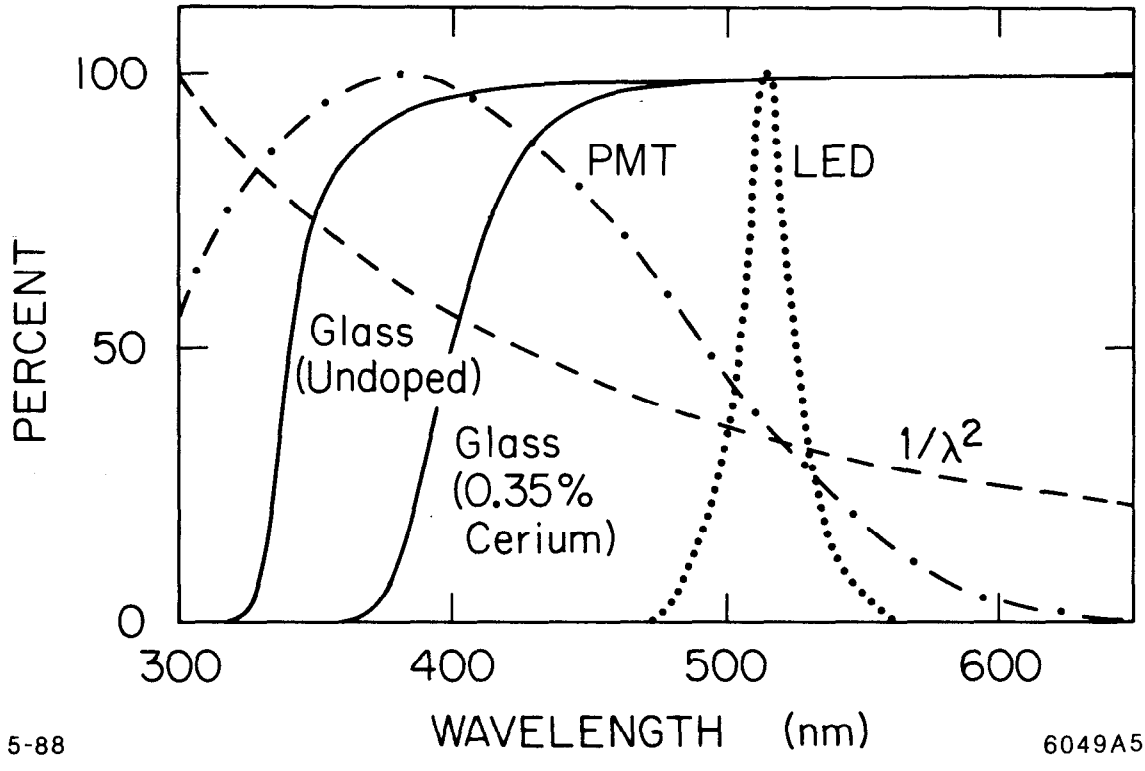
100
50
0
PERCENT
PMT
LED
Glass
(Undoped)
Glass
(0.35%
Cerium)
1/λ²
300
400
500
600
WAVELENGTH (nm)
5-88
6049A5

Fig. 6

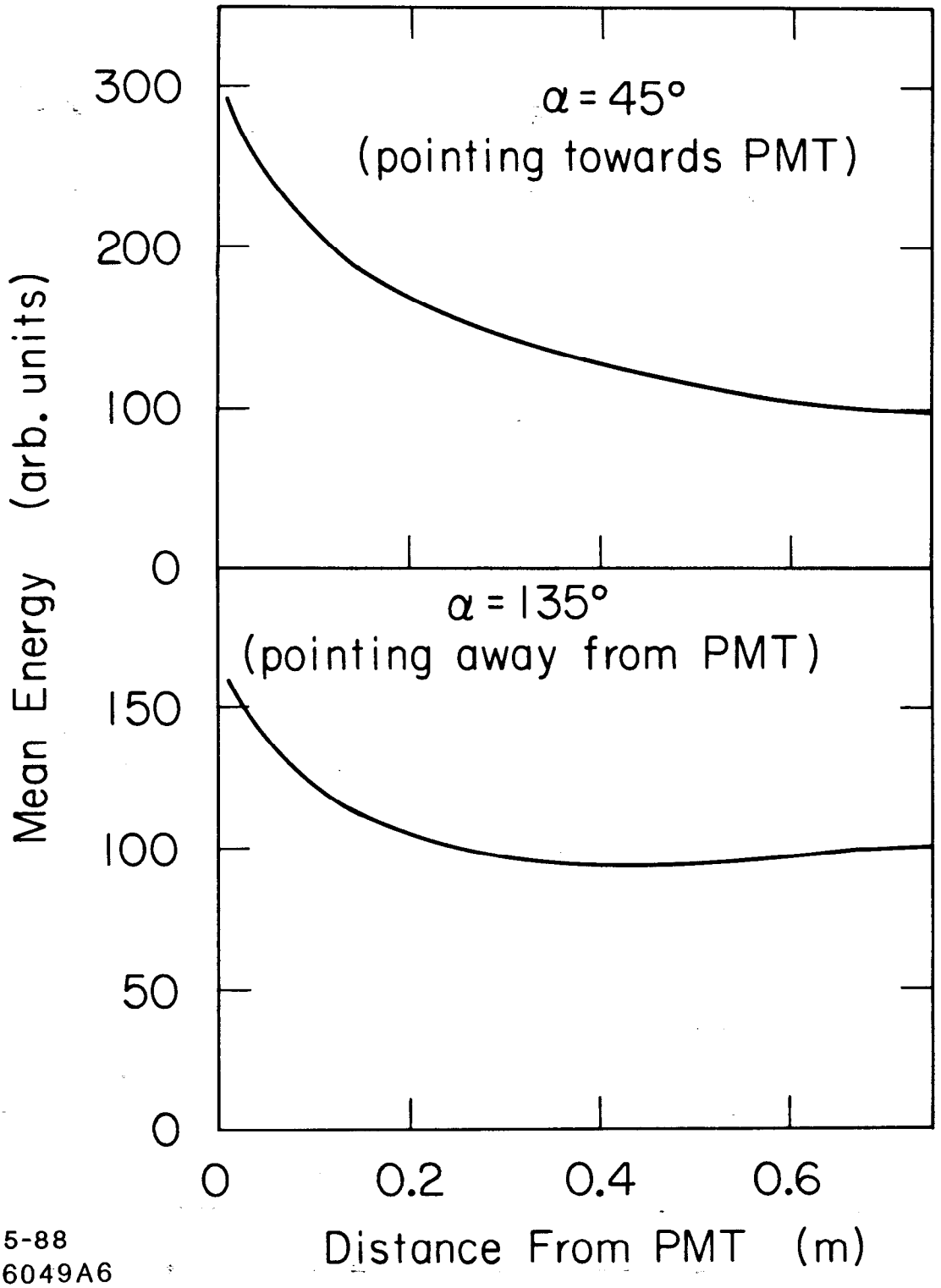

5-88
6049A6

Fig. 7

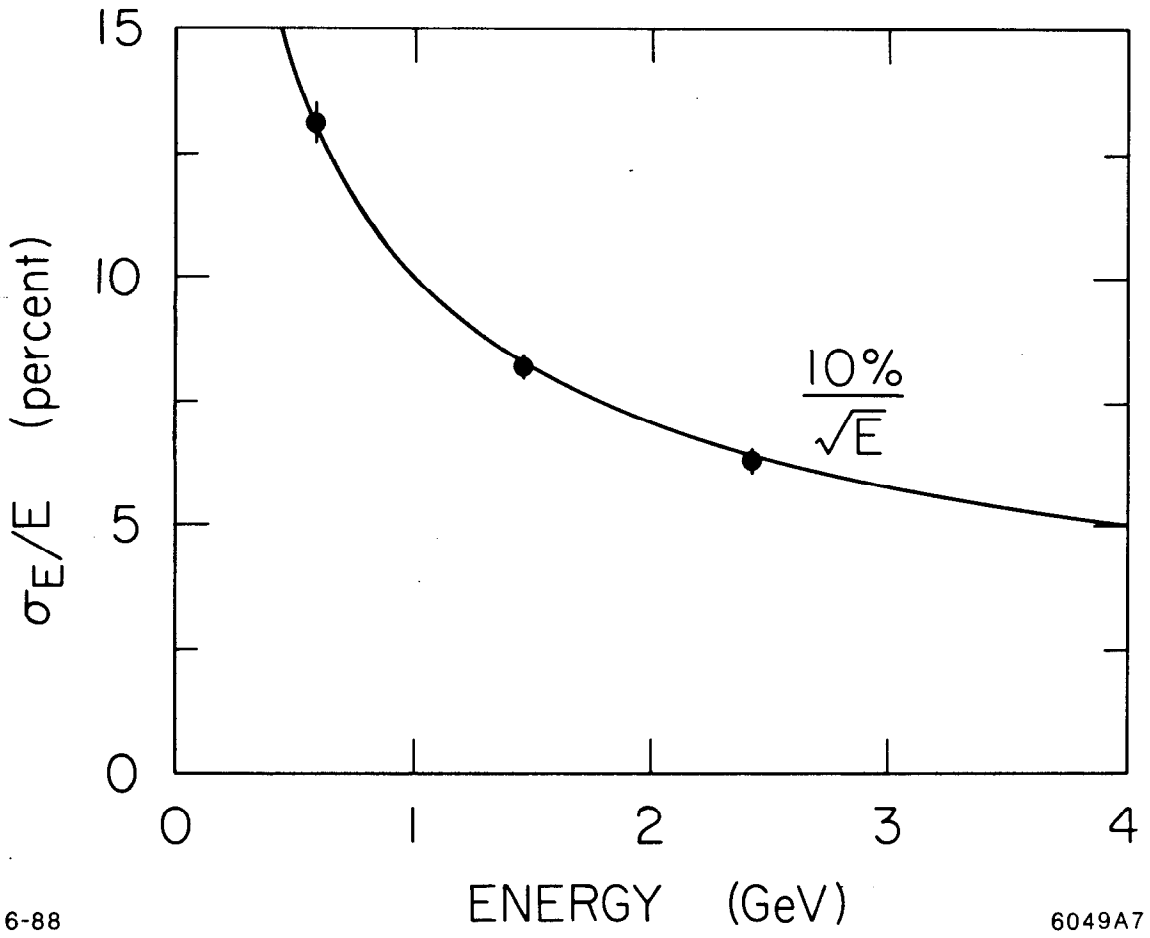
15
10
5
0
σ_E/E (percent)
10%
$\sqrt{E}$
0
1
2
3
4
ENERGY (GeV)
6-88
6049A7

Fig. 8

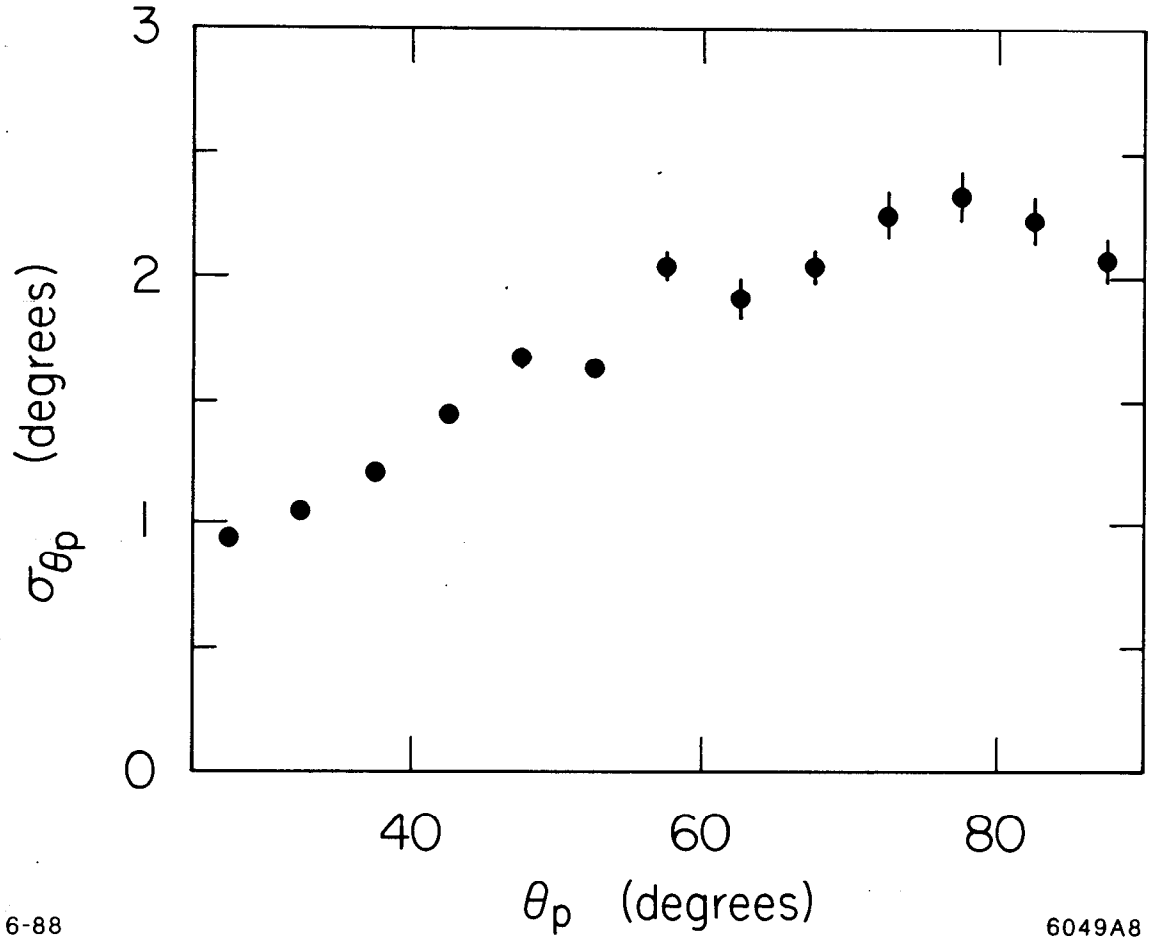
3
2
1
0
σ_{θ_p} (degrees)
40
60
80
θ_p (degrees)
6-88
6049A8

Fig. 9

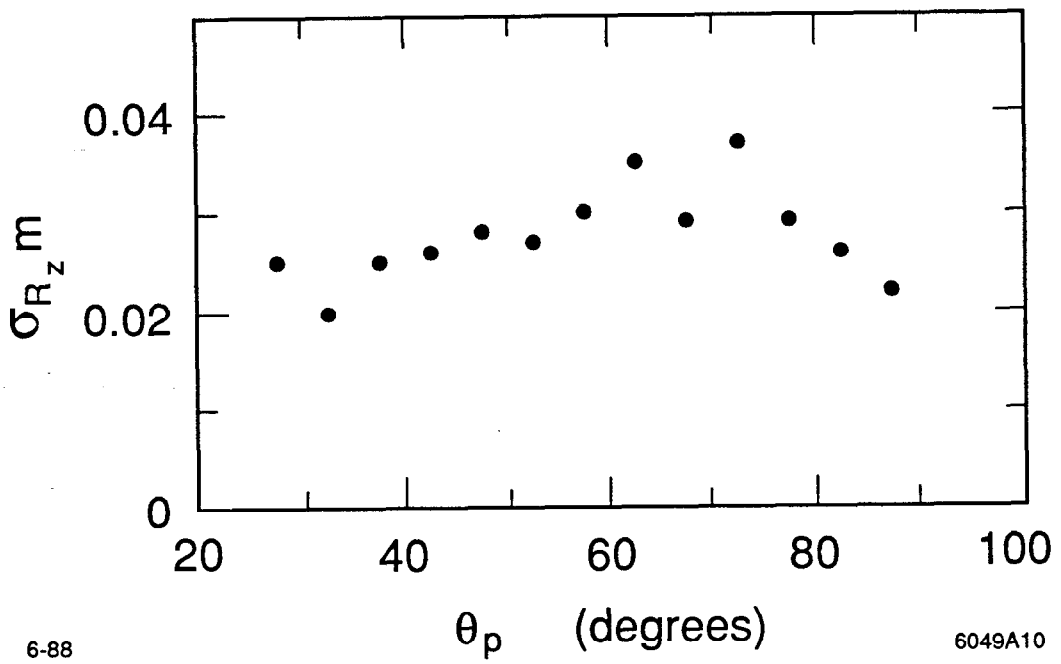

Fig. 10

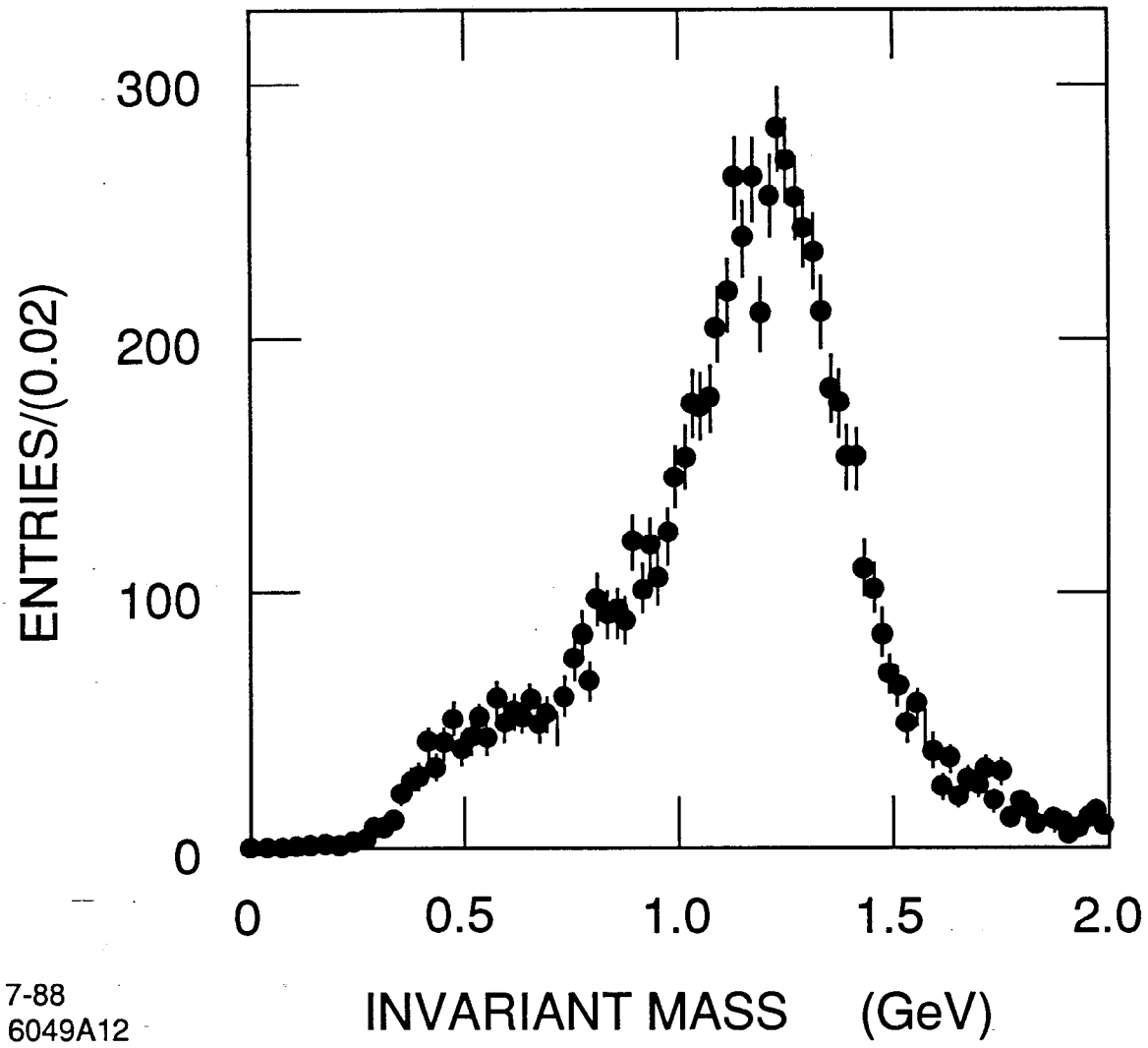

7-88
6049A12

Fig. 11

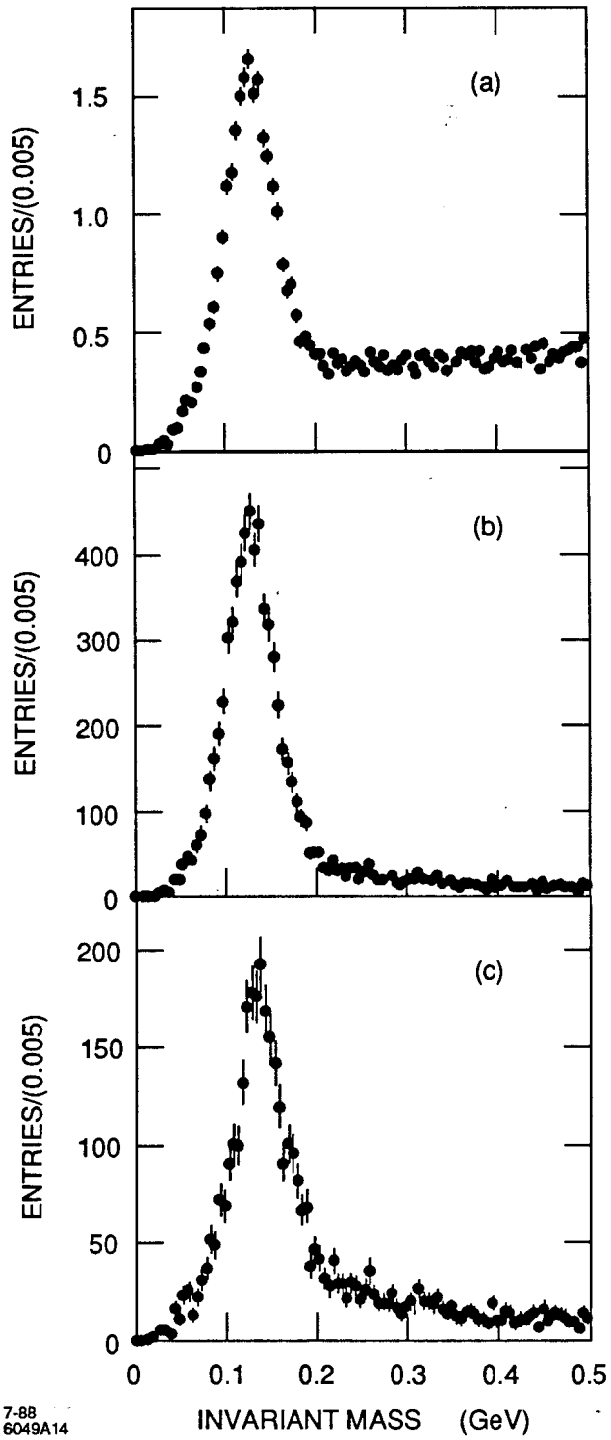
(a)
(b)
(c)
ENTRIES/(0.005)
ENTRIES/(0.005)
ENTRIES/(0.005)
1.5
1.0
0.5
0
400
300
200
100
0
200
150
100
50
0
0
0.1
0.2
0.3
0.4
0.5
INVARIANT MASS (GeV)
7-88
6049A14

Fig. 12

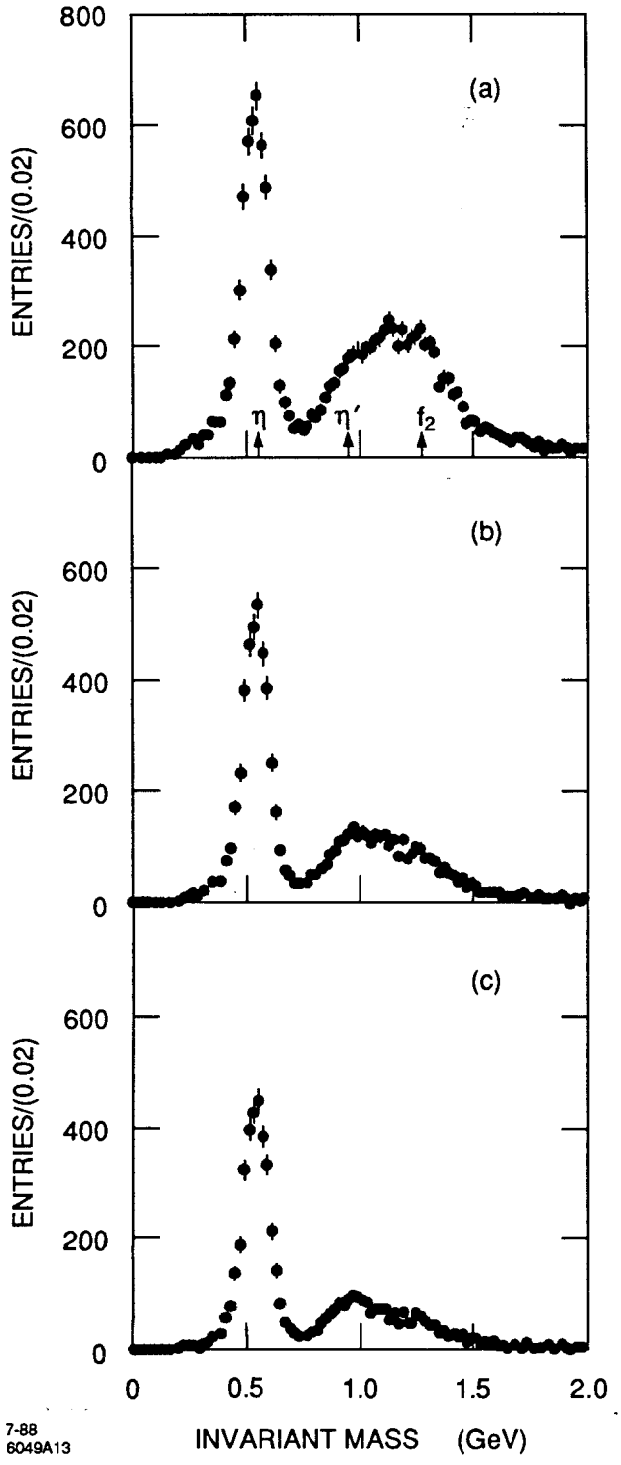
800
600
400
200
0
ENTRIES/(0.02)
(a)
η
η′
f2
(b)
(c)
0
0.5
1.0
1.5
2.0
INVARIANT MASS (GeV)
7-88
6049A13

Fig. 13

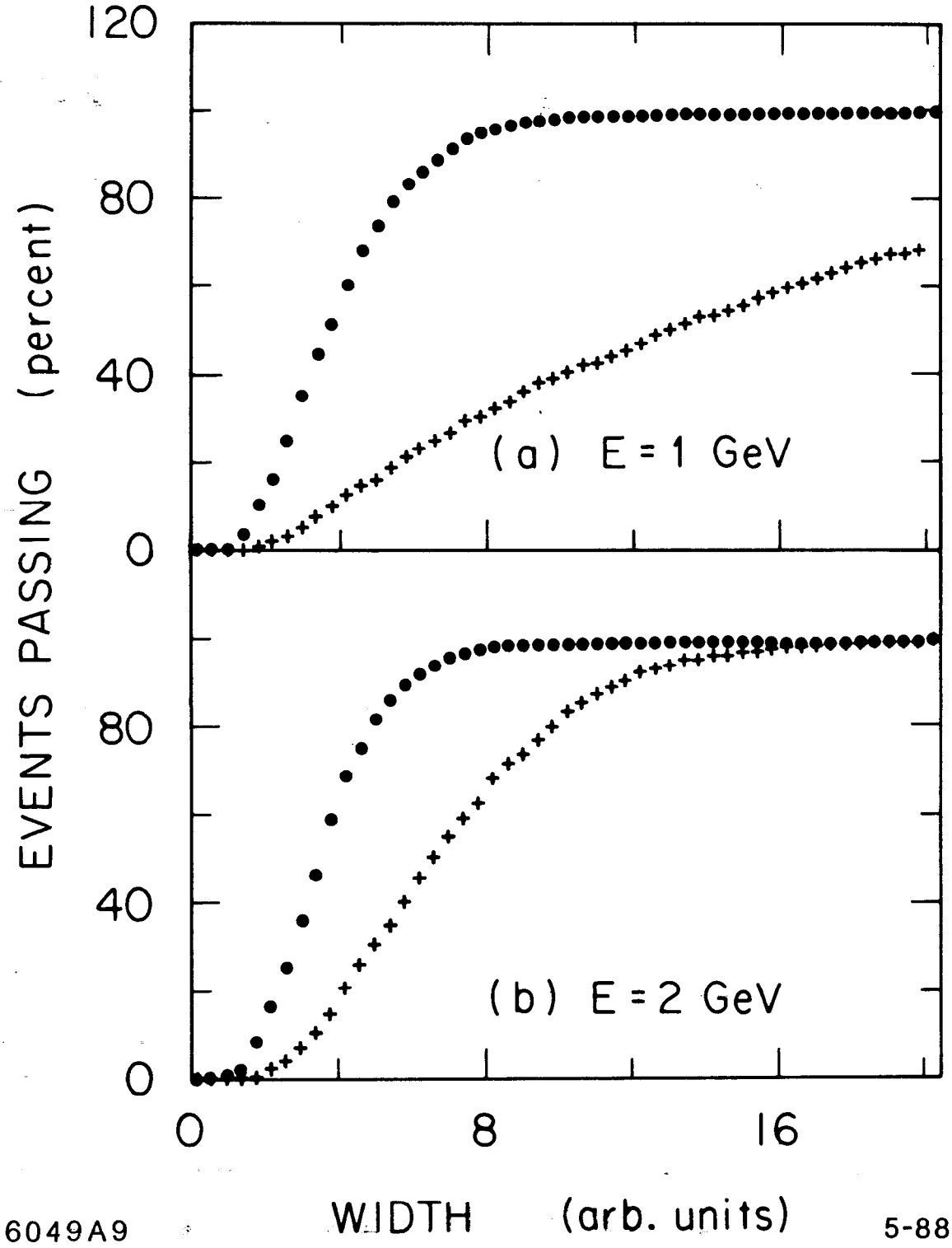

6049A9

5-88

Fig. 14